Review

Evangelos Th. Papaioannou* and René Beigang

THz spintronic emitters: a review on achievements and future challenges

https://doi.org/10.1515/nanoph-2020-0563
Received October 8, 2020; accepted November 26, 2020; published online December 18, 2020

Abstract: The field of THz spintronics is a novel direction in the research field of nanomagnetism and spintronics that combines magnetism with optical physics and ultrafast photonics. The experimental scheme of the field involves the use of femtosecond laser pulses to trigger ultrafast spin and charge dynamics in thin films composed of ferromagnetic and nonmagnetic thin layers, where the nonmagnetic layer features a strong spin–orbit coupling. The technological and scientific key challenges of THz spintronic emitters are to increase their intensity and to shape the frequency bandwidth. To achieve the control of the source of the radiation, namely the transport of the ultrafast spin current is required. In this review, we address the generation, detection, efficiency and the future perspectives of THz emitters. We present the state-of-the-art of efficient emission in terms of materials, geometrical stack, interface quality and patterning. The impressive so far results hold the promise for new generation of THz physics based on spintronic emitters.

Keywords: optospintronics; spintronics; THz spintronics; ultrafast photonics.

PACS: 85.75.d; 75.78.Jp; 75.76.+j.

1 Introduction

Terahertz (THz) radiation covers a broad bandwidth of the electromagnetic spectrum from 100 GHz to 30 THz [1] lying between the microwave and the far infrared band. THz radiation is utilized by a number of scientific and research communities, ranging from chemistry and medicine to physics and material sciences. Recent technological innovations in optics and photonics enable THz research and technology to address an increasingly wide variety of applications [2, 3]: information and communications technology; spectroscopy and imaging, biology, medical and pharmaceutical sciences; nondestructive evaluation (material and circuitry diagnosis), security (detection of drugs and explosives), global environmental monitoring, THz sensor networks, ultrafast computing and astrophysics. Despite all that, the THz region of the electromagnetic spectrum is still an comparatively unexplored region due to the lack of strong and broadband THz emission sources and sensitive detectors.

Here, we review the recent developments in nanomagnetism and spintronics that allowed the first usage of ultrafast spin physics for THz emission. The physical mechanism of the THz radiation of spintronic emitters is based on the inverse spin Hall effect [4] and appears in multilayer heterostructures that consist of ferromagnetic (FM) and nonmagnetic (NM), usually heavy metal, layers. When illuminated by ultrafast femtosecond (fs) laser pulses, spin-polarized electrons are excited in the FM layer and subsequently diffuse as a spin current into the NM layer. Due to the inverse spin Hall effect (ISHE), the spin current is converted into a transient transverse charge current in the NM layer resulting in THz emission [4]. This new source of THz radiation is an emerging topic subject to intensive research. The efficiency of such emitters is in some cases comparable with established types of THz sources (for example, with nonlinear crystals) [5]. The engineering of THz emission is the main technological and scientific challenge and is currently the target of many research activities. In this review article, we highlight and examine the different strategies that have been followed in order to explore the properties of the emitted THz signal, like THz amplitude and bandwidth, e.g., different material compositions of FM/NM systems with a variety of thicknesses, spintronic emitters in different geometrical stacking order using different layers and patterned structures, different substrates, interface materials and quality of

***Corresponding author: Evangelos Th. Papaioannou**, Institute of Physics, Martin-Luther University Halle-Wittenberg, 06120 Halle, Germany, E-mail: evangelos.papaioannou@physik.uni-halle.de. https://orcid.org/0000-0002-9822-2343
René Beigang, Department of Physics, Technische Universität Kaiserslautern, 67663 Kaiserslautern, Germany, E-mail: beigang@physik.uni-kl.de

interfaces and dependence on the excitation wavelength. First, we highlight the radiation mechanism and the experimental way to measure the emitted THz radiation. We explore the current trends to engineer the properties of the THz emission and we discuss the future challenges to integrate spintronic emitters in THz devices. We finally explore the potential of the emitter to extend the THz field and widen its applications. The reader should notice that this work summarizes only experimental results from the last couple of years and does not review theoretical models and calculations of the spin transport in magnetic heterostructures. In addition, we focus on the mechanism of THz generation from the ISHE and we will not deal in depth with other novel sources of THz radiation originating from other mechanisms like anomalous Hall effect or Rashba interfaces, since both are much less effective as THz sources compared to the ISHE mechanism.

2 Description of the spin-to-charge conversion mechanism responsible for the THz radiation

Commonly, optically generated THz radiation is based on either transient photocurrents in semiconductors induced by ultrashort optical pulses from femtosecond lasers or by utilizing nonlinear optical responses of bound electrons in nonlinear crystals [1, 6]. The source of the THz radiation is the time-varying photocurrent in semiconductors (photoconductive switches PCA) or time-varying polarization in electro-optical crystals (nonlinear optical methods). Further, THz radiation can be obtained from free electrons in vacuum either from a bunch of relativistic electrons or from periodically undulated electron beams [1, 6]. Besides the aforementioned physical principles for the THz radiation, which are known as electric dipole emission, a time-varying magnetization on the ultrafast, (sub)-picosecond timescale can also act as a THz source, the so-called magnetic dipole emission. Such emission was first observed from optically excited magnetic metallic structures during the ultrafast demagnetization process of the magnetic layers [7, 8]. This type of radiation is weak due to its magnetic dipole character.

For all these methods, there are limitations concerning the generated intensities and/or the available bandwidth. The use of PCAs is, in general, limited to low power excitation sources and, as a consequence, to low intensities of the generated THz pulses. The bandwidth is usually governed by material properties (intrinsic phonon absorption in the materials used) and typically ends around 8 THz. In addition, fabrication of PCAs requires an advanced technology to obtain, e.g., the correct structuring which significantly determines the desired properties. Nonlinear methods are, in principle, well suited for THz generation. However, in order to achieve phase matching only very short nonlinear crystals in combination with ultrashort laser pulses can be used to obtain a decent bandwidth. This in turn limits the intensity of the generated THz pulses. The use of high power excitation sources is limited by the damage threshold of the nonlinear crystals.

In contrast, for THz generation in spintronic THz emitters the physical mechanism is different and is based on the excitation of a spin current and the inverse spin Hall effect (ISHE), Figure 1. A femtosecond laser pulse pumps a FM/NM heterostructure and leads to a spin-dependent excitation of electrons in the FM layer. Subsequently, these electrons are diffused in the nonmagnetic layer through a super diffusive process [4, 9]. This longitudinal spin-polarized charge current is then converted into a transient transverse charge current due to the ISHE in the NM layer. The spin current induces an effective charge current perpendicular to itself and the magnetization axis according to:

$$\mathbf{j}_c = \Theta_{\mathrm{SH}}\, \mathbf{j}_s \times \frac{\mathbf{M}}{|\mathbf{M}|}\,, \tag{1}$$

where the spin Hall angle is denoted by Θ_{SH}. Here, it is assumed that the magnetization points in positive x-direction, j_c as magnitude in y-direction and j_s in z-direction, along the layer stacking (Figure 1).

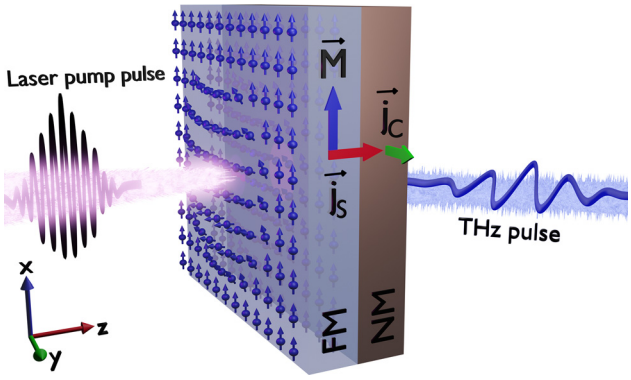

Figure 1: Graphical representation of the THz emission from FM/NM heterostructures after fs-laser excitation of the spin system. The magnetization points in positive x-direction, j_s is the spin current in z-direction, along the layer stacking and j_c is the charge current in y-direction. The inverse spin Hall effect leads to the THz radiation. The polarization of the THz field is perpendicular to the direction of the magnetic field.

The transient charge current generates a short terahertz pulse that propagates perpendicular to the electrical current. The origin of the THz radiation is the evolution of the hot-carrier distribution after the femtosecond laser excitation. The emission is dominated by the electric dipole emission driven by a time varying ISHE-type electric current [4, 5]. Theoretically, the Boltzmann transport theory has been proven to be an adequate tool to simulate excited carrier dynamics in metallic structures on the nanoscale [4, 9–12], however, in this review, the theoretical approaches are out of the focus.

The shape of the experimentally obtained pulses and their corresponding spectra depend on the experimental THz-setup and is a convolution of emitter and detector response. The measured bandwidth, for example, reaches 8 THz in the study by Torosyan et al. [13], which is mainly limited by the detector response which is a low temperature (LT)-GaAs photoconductive antenna in this case. Bandwidths with full-width at half-maximum (FWHM) up to 30 THz measured with electro-optical sampling and faster excitation pulses were reported [5].

It is worth to mention here that the origin of the THz emission after fs-laser excitation is difficult to disentangle between ISHE-type and laser-driven transient demagnetization in the magnetic layers. Recently, Zhang et al. [14] successfully separated and measured the weak THz emission during the demagnetization process, suggesting to implement this type of weak THz emission for ultrafast magnetometry on a pico- and sub-pico timescales. Presently, new spin-to-charge-conversion mechanisms have been proposed as sources of THz radiation. One is the THz emission from Rashba-type interfaces [15, 16] where the generation of THz waves takes place at interfaces between two nonmagnetic materials due the inverse Rashba Edelstein effect. In a similar experimental procedure, the fs-laser pulse induces a nonequilibrium electron flow in FM/Ag/Bi heterostructures. A femtosecond spin current pulse is launched in the ferromagnetic $Co_{20}Fe_{60}B_{20}$ layer and drives terahertz transients at a Rashba interface between two nonmagnetic layers, Ag and Bi. In contrast to the THz emission in spintronic emitters via the inverse spin Hall effect, the inverse Rashba Edelstein effect transforms a nonzero spin density induced by the spin current injection into a charge current carried by interfacial states. Another alternative mechanism for generating THz emission from an ultrathin FM layer via the anomalous Hall effect was recently proposed [17]. The process involves a single FM layer and the generation of backflow superdiffusive currents at the dielectric/FM/dielectric interfaces and subsequent conversion of the charge current to transverse current due to the anomalous Hall effect. The THz generation is suggested to be mainly caused by the nonthermal superdiffusive current near the two FM/dielectric interfaces.

3 Experimental detection of THz emission from spintronic emitters

Detection of the emitted THz pulses from spintronic emitters is often accomplished with the established terahertz time-domain spectroscopy (THz-TDS) system [18]. A specific example is presented in Figure 2. The system is driven by a femtosecond laser delivering sub-100 fs optical pulses at a repetition rate of usually 50 to 100 MHz with an average output power of typically 600 mW. The laser beam is split into a pump and probe beam usually by a 90:10 beamsplitter. The stronger part is led through a mechanical computer-controlled delay line to pump the THz emitter, and the weaker part is used to gate the detector, a photoconductive switch with a dipole antenna of specific dimensions. In our example here, we refer to a 20 μm dipole antenna. In a classical (standard) THz setup, both the emitter and the detector operate with photoconductive antennas (PCA), whereas in the case of spintronic emitters the PCA emitter is substituted by the spintronic sample, which is placed in a weak magnetic (a few mT) field perpendicular to the direction of the pump beam and usually in the direction of the easy axis of magnetic layer in order to achieve saturation. The direction of the magnetic field determines the polarization of the THz field, which is perpendicular to the direction of the magnetic field. Changing the direction of magnetic field into the opposite direction changes the phase of the detected THz waveforms by 180° (Figure 2b). In this way, by changing the orientation of the magnetic field the polarization of the generated THz radiation can be changed easily.

The optical pump beam, that is sharply focused onto the sample at normal incidence by an aspherical short-focus lens, excites spin-polarized electrons in the magnetic layer (Fe), which give rise to a spin current, which in turn excites a transverse transient electric current in the Pt layer. The latter results in THz pulse generation of sub-picosecond duration being emitted forward and backward into free space in the form of a strongly divergent beam. The central wavelength within the beam is about 200 μm and is much longer than the diameter of its source, which is smaller than 10 μm. That is why the emitted THz field fills the half-space behind the sample. A strategy to increase the collection efficiency was used by Torosyan et al. [13], comparable to techniques familiar with

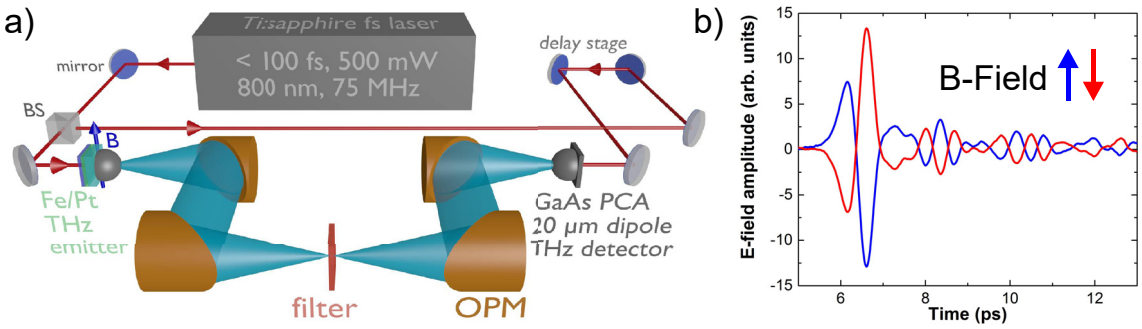

Figure 2: a) An example of a terahertz time-domain spectroscopy (THz-TDS) experimental setup modified for spintronic emitters. b) THz pulses for two opposite directions of the magnetic field.

photoconductive antenna setups: a hyperhemispherical Si lens was attached at the back side of the sample, able to collect the divergent beam in the form of a cone and direct it further. With the lens attached an enhancement factor of up to 30 in electric field amplitude has been reported [13]. After that the beam is collimated with an off-axis parabolic mirror and sent to an identical parabolic mirror in the reversed configuration. The latter focuses the beam to the second Si lens, which finally focuses the beam through the GaAs substrate of the detector PCA onto the dipole gap for detection. In this way, the THz optical system consisting of the two Si-lenses and the two parabolic mirrors images the point source of THz wave on the emitter surface onto the gap of the detector PCA and ensures an efficient transfer of the emitted THz emission from its source to the detector. In addition to having two collimated beam paths, this 4-mirror THz-optics also allows for an intermediate focus of the THz beam aimed at imaging applications (Figure 2a).

In such configuration, the THz beam path is determined by the silicon lens on the emitter, the parabolic mirrors and the silicon lens on the photoconducting antenna of the detector. The alignment of these components is not changed during an exchange of the spintronic emitter. If in addition the position of the pump beam focus remains constant, the spintronic emitter can easily be exchanged without changing the beam path, as the lateral position of the focus on the emitter is not critical assuming a homogeneous lateral layer structure. The frequency response of the photoconductive dipole antenna with 20 µm dipole length limits the observable bandwidth. With this dipole length, a maximum detector response of around 1 THz can be expected with a reduction to 50% at 330 GHz and 2 THz. The 10% values are at 100 GHz and 3 THz [19]. In fact, the detected signal is strongly influenced by the detector response. The frequency response of the photoconductive antenna-detector above 3 THz is very flat and at 8 THz a strong phonon resonance in GaAs, which is used as substrate material for the photoconductive antenna, causes strong absorption of the THz radiation. Above 8 THz, almost no THz radiation can be detected. The delay line provides the synchronous arrival of the weaker part of the optical pulse and that of the THz pulse at the detector antenna gap from either side, as well as the scanning in time, the so-called open state of the gap along the THz pulse duration. In each position of the delay line, the transient current induced in the detector by the electric field of the THz sub-picosecond pulse is proportional to its instantaneous electrical field value. It is summed up from many laser pulses, which reach the detector during the single step of the delay line, and it is integrated within the "open" state time window. It is measured as one single point of the THz wave-form and is in the order of several nanoamperes at the maximum of the THz pulse. Hence, a lock-in technique has to be used. For that purpose, the pump beam is mechanically chopped at usually kHz frequency. By scanning the "open" state of the detector in time, the THz pulse shape can be sampled. Utilizing the magnetic field dependence of the THz polarization the THz beam can, in principle, also be chopped electrically by means of an alternating magnetic field around the emitter.

Alternatively, free-space electro-optical sampling (EOS) is used for the detection of THz radiation from spintronic emitters [20, 21]. In order to be able to detect frequencies well above 10 THz very thin ZnTe crystals are used as a detector in combination with extremely short laser pulses. The ease of implementation and the possibility to detect higher bandwidths [5] render this technique

also popular for the investigation of the efficiency of the magnetic heterostructures.

4 Strategies to engineer intensity and frequency bandwidth of the emitted THz signal

Currently, the main goal of the research on spintronic emitters is the engineering of THz emission and different strategies have been followed in order to explore the THz amplitude and bandwidth of the signal. In Figure 3 we construct a roadmap with the most important physical parameters, which can influence the efficiency of the spintronic THz-emitters toward higher signal strengths and broader bandwidths. Figure 3 summarizes all the important factors that can affect the temporal and spatial evolution of the spin current inside the metallic layers, by taking into account, the generation and optical propagation of the THz wave, and forecasts the THz-pulse shapes and spectra, by taking into consideration the electron scattering lifetime and the interfacial spin current transport. Parameters that are included in Figure 3 and play a decisive role in the emission are: Θ_{SH} is the spin Hall angle, λ_{SD} is the spin-diffusion-length, T is the interface transmission parameter and τ_{el} is the inelastic scattering lifetime. Moreover, included in the roadmap are effects originating from the excitation wavelength, from geometrical stacking order, from the FM and NM layer thickness t_{FM}, t_{NM} and electrical conductance σ_{FM}, σ_{FM}, and from the index of refraction and the absorption coefficient of all involved layers (metals and insulators) in the THz-range n_i and κ_i. Theoretical calculations and simulation of the spin current transport with the Boltzmann equation and of the optical path with the use of the transfer matrix for the total layer stack M_{tot} are also necessary tools for the understanding and the evaluation of the research progress.

The following sections will analyze the roadmap by reviewing the research efforts on different material compositions, geometrical factors, interfaces and nanopatterning. We will present key works and summarize the unique advantages and the promises for applications of spintronic emitters to the development of THz technology.

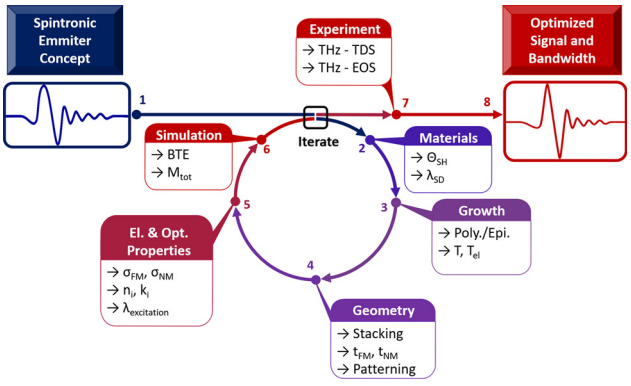

Figure 3: Roadmap to efficient spintronic THz-emitters with high signal strength and broad bandwidth. Here, Θ_{SH} is the spin Hall angle, λ_{SD} is the spin-diffusion length, T and τ_{el} are the interface transmission parameter and the elastic scattering lifetime, respectively. t_{FM}, t_{NM}, σ_{FM} and σ_{FM} are the FM and NM layer thickness and electrical conductance, respectively. n_i and κ_i are the index of refraction and the absorption coefficient of all involved layers (metals and insulators) in the THz range, respectively. $\lambda_{excitation}$ is the wavelength of the laser excitation. BTE refers to the Boltzmann transport equation, M_{tot} is the transfer matrix used to describe the propagation of the generated THz wave throughout the total layer stack. THz-detection schemes are defined as THz-TDS for the time domain spectroscopy and THz-EOS for the free space electro-optical sampling. Figure modified from the study by Nenno et al. [22].

4.1 Material dependence

A variety of materials combination of ferromagnetic (FM)/nonmagnetic (NM) layer systems have been so far explored as spintronic emitters. We initially focus on the choice of the magnetic layer. Direct comparison between the 3d metals like Fe, Co and Ni, in structures like FM (3 nm)/Pt (3 nm) [5] and in FM (2 nm)/Pt (5 nm) [23] have revealed that Ni yields the lowest signal with Fe having a slightly higher signal than Co. The comparison of ferromagnetic alloys like $Ni_{89}Fe_{19}$, $Co_{70}Fe_{30}$, $Co_{40}Fe_{40}B_{20}$ and $Co_{20}Fe_{60}B_{20}$/Pt (3 nm) [5] showed the prominent role of the CoFeB alloy. Sasaki et al. [24] varied the composition of Co and Fe in the CoFeB alloy. They found that the THz emission in $Ta/(Co_xFe_{1-x})_{80}B_{20}$ is enhanced at compositions of approximately $x = 0.1–0.3$ which show a maximum saturation magnetization. Modification of the magnetic layer with ferrimagnetic gadolinium and terbium-iron alloys was achieved by Schneider et al. [25, 26]. Both systems Gd_xFe_{1-x}/Pt and Tb_xFe_{1-x}/Pt present the highest THz emission for small rare-earth content. However, the Gd_xFe_{1-x} exhibit up to 17 times higher amplitudes. A strong THz output was observed from compensated ferrimagnetic $Co_{1-x}Gd_x$ (7 nm)/Pt (6 nm) bilayers. The THz signal decreases as the Gd fraction increases. At the compensation point for $x = 26$, the almost zero net magnetization was not strongly correlated to the emitted THz signal [20]. The replacement of the ferromagnetic layer with $DyCo_5$, $Gd_{24}Fe_{76}$, Fe_3O_4 and FeRh showed that they exhibit lower

THz emission with respect to CoFeB layer [27]. Furthermore, Co-based Heusler alloys and in particular Co_2MnSi (CMS) was investigated as spin injector in CMS/Pt bilayers [28]. The achievement of the highly ordered B2 structural phase after annealing led to up to two times higher THz emission compared to CoFe/Pt bilayers. The effect was attributed to the small conductivity and the comparable to FeCo spin current injection of the CMS samples.

The efficiency of the conversion of spin-to-charge current is quantified by the spin Hall angle and the spin current relaxation length of the nonmagnetic layer. Different nonmagnetic materials have been studied so far for THz emission. The THz signal amplitude seems to scale with the intrinsic spin Hall conductivity of the used NM layer [5], see Figure 4. The THz emission was even used to estimate the relative spin Hall angle [21, 29]. The prominent choice at the moment is Pt since it has provided so far the highest signal compared to W [21], $Cu_{80}Ir_{20}$ [21], Ta [29], Ru [29, 30], Ir [29], Pd [30], $Pt_{38}Mn_{62}$ [5]. Interestingly, NM layers with opposite sign of the spin Hall angle compared to Pt give rise to THz signals with opposite polarities and subsequently confirm the ISHE origin of the THz emission.

The spin-to-charge-conversion mechanism driven by the spin Seebeck effect was additionally probed in insulating magnetic/NM interfaces like YIG/$Cu_{1-x}Ir_x$ [31] and YIG/Pt [32] showing, however, much lower efficiency of the THz emission compared to the metallic magnetic layers.

4.1.1 Material dependence—summary and outlook

According to experiments performed up to now bilayers composed of CoFeB/Pt and Fe/Pt provide the highest THz signal and they are the most prominent material choices so far. Other classes of magnetic layers have been also studied like compensated ferrimagnets, Heusler alloys, insulating ferrimagnets like YIG, however, their efficiency is low. Novel capping materials as spin-to-charge converters like at ferromagnetic/semiconductor interface [33], and topological insulators with large spin Hall angle like BiSe [34] used in combination with FM layers as in Bi_2Se_3/Co interface [35] can promote large spin injection efficiency, and pave the way for future investigations on materials.

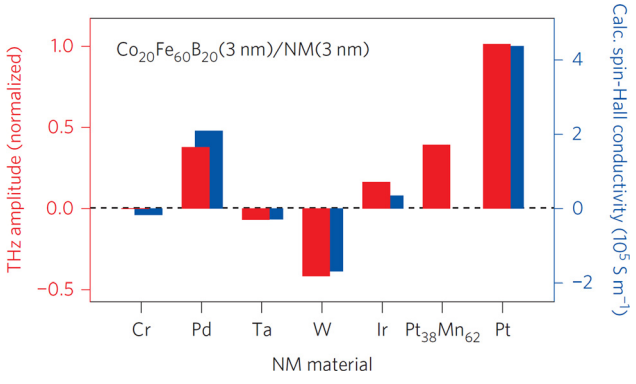

Figure 4: Spin Hall angle and spin Hall conductivity for the nonmagnetic (NM) layer. Pt has so far the highest efficiency for THz emission. Reprinted by permission from Springer Nature, Nature Photonics, T. Seifert et al. [5] Copyright 2016.

4.2 Thickness dependence

Various thickness dependence studies on the efficiency of the THz emission have revealed the critical role of the thicknesses of the individual layers. Studies on the variation of the thickness of the NM-layer and by keeping constant the thickness of the FM layer have shown the existence of an optimum thickness around 2–3 nm [13]. This range of thicknesses holds for different NM-layers like Pt [21, 29, 13], W [21, 29] where the maximum signal is obtained, see Figure 5. By fitting the NM-thickness dependence of the THz amplitude, the spin current diffusion length was extracted [21, 13]. Surprisingly, the latter was found to agree with values extracted from GHz spin pumping experiments although the excitation of the spin current is performed in different time- and energy scales. The physical mechanism behind this similarity is currently under on-going research [36].

In the same way, for a constant NM-layer thickness, there is an optimum FM layer thickness in the same range of about 2–3 nm [21, 29, 13]. When the ferromagnetic layer is too thin, then either the loss of magnetic order due to heating effects or the reorientation of the magnetization due to monolayer thickness cause a drastic reduction of the THz signal. The theory of the effect of changing layer thickness was first developed in the study by Seifert et al. [5] for detection of THz-signal from NM-layer side. A further expansion of the model was achieved in the study Torosyan et al. [13], and it is expressed by Eq. (2). The equation holds when the fs-laser illuminates first the NM-layer side and the detection is performed after the THz-signal has travelled through the substrate (see also the study by Torosyan et al. [13]):

$$E_{\mathrm{THz}} \propto \Theta_{\mathrm{SH}} \frac{P_{\mathrm{abs}}}{d_{\mathrm{Fe}} + d_{\mathrm{Pt}}} \cdot \tanh\left(\frac{d_{\mathrm{Fe}} - d_0}{2\lambda_{\mathrm{pol}}}\right) \cdot \frac{1}{n_{\mathrm{air}} + n_{\mathrm{Sub}} + Z_0 \cdot (\sigma_{\mathrm{Fe}} d_{\mathrm{Fe}} + \sigma_{\mathrm{Pt}} d_{\mathrm{Pt}})} \cdot \tanh\left(\frac{d_{\mathrm{Pt}}}{2\lambda_{\mathrm{Pt}}}\right) \cdot e^{-(d_{\mathrm{Fe}}+d_{\mathrm{Pt}})/s_{\mathrm{THz}}} \tag{2}$$

where n_{air}, n_{Sub} and Z_0 are the index of refraction of air, the index of refraction of the substrate at THz frequencies and the impedance of vacuum, respectively. Equation (2) takes into account all successive effects that take place, after the laser pulse impinges on the bilayer. In particular, the first term contains the spin Hall angle, the second term accounts for the absorption of the femtosecond laser pulse in the metal layers. As only spin-polarized electrons within a certain distance from the boundary between FM and NM will reach the NM layer, only a fraction of the measured total absorbed power contributes to the generated THz signal. This fraction scales with the inverse of the total metal layer thickness $1/(d_{Fe} + d_{Pt})$. The third term describes generation and diffusion of the generated spin current flowing in FM toward the interface with NM. The possibility that extra thin FM layers can lose their ferromagnetic properties below a certain thickness can be captured by introducing the term d_0 in Eq. (2). Below this critical thickness, it is considered that the flow (if any) of spin current in FM does not reach the NM layer. Above this critical thickness, the generated spin polarization saturates with a characteristic constant λ_{pol}. The fourth and fifth terms, the tangent hyberbolic function divided by the total impedance, refer to the spin accumulation in Pt, which is responsible for the strength of the THz radiation and it depends on the finite diffusion length λ_{Pt} of the spin current in NM layer. The symbols σ_{Fe} and σ_{Pt} correspond to the electrical conductivities of the layers. This part of the equation also includes the shunting effect of the parallel connection of the resistances of the individual FM and NM layers. The last term describes the attenuation of the THz radiation during propagation through the metal layers (with s_{THz} as an effective inverse attenuation coefficient of THz radiation in the two metal layers. The last term is required since as aforementioned, the sample is excited from the outer Pt side, whereas the THz radiation is collected behind the substrate, thus propagating through both metal layers [13]. In the case of small losses, the attenuation can be taken into account by this single exponential factor and the fourth factor, which accounts for the multiple reflections of the THz pulse at the metal/dielectric interfaces. All terms together describe the layer thickness dependence of the measured THz amplitudes.

Furthermore, additional factors have been proposed to influence the thickness dependence like the factor of interfacial spin memory loss [37] in Co/Pt bilayers.

4.2.1 Thickness dependence—summary and outlook

The behavior of the thickness dependence of the THz signal from spintronic emitters is established. In general, the optimal thickness of the NM layer depends in particular on the spin diffusion length. For thicknesses larger than the spin diffusion length, the signal is reduced. For very thin

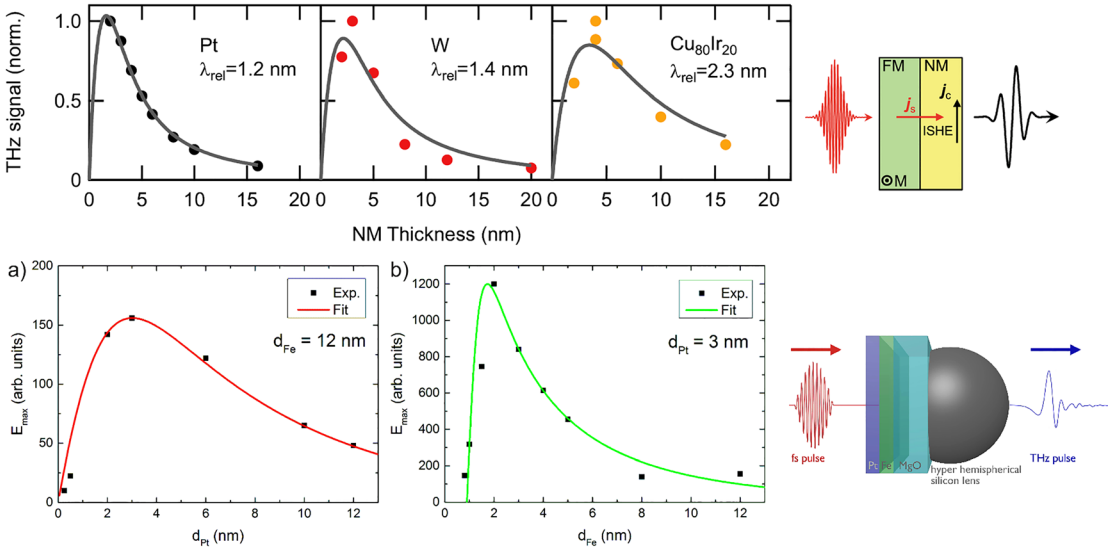

Figure 5: (Upper panel) Nonmagnetic layer thickness dependence of THz emission for different NM layers like Pt, W, CuIr in CoFeB/NM bilayers [21], and the geometrical arrangement of the experiment. Reproduced under the terms of a Creative Commons Attribution 3.0 Licence [21], 2018 IOP Publishing Ltd.
(Lower panel) (a) Pt thickness dependence of the THz field amplitude for a constant Fe thickness of 12 nm. (b) Fe thickness dependence of the THz field amplitude for a constant Pt thickness of 3 nm [13]. The geometrical arrangement is also depicted to the right of the graph. Reproduced under a Creative Commons Attribution 4.0 International License [13], The Authors 2018, published by Springer Nature.

magnetic layers, the change of the magnetic order also reduces the THz emission. Future studies on the thickness dependence will aim to study the effect in complex multilayer structures. Of large interest are the investigations and the comparison on spin current diffusion length for ultrafast fs-laser excitation and microwaves (GHz) excitation schemes.

4.3 Wavelength dependence

The majority of the experiments up to now with spintronic THz emitters are performed at 800 nm excitation wavelength using femtosecond Ti:sapphire lasers. Would different excitation energies of the incoming fs-laser pulses influence the spin current dynamics and subsequently the THz-emission? Recent investigations have tried to answer this question using different excitation wavelengths. Papaioannou et al. [38], used an optimized spintronic bilayer structure of 2 nm Fe and 3 nm Pt grown on 500 μm MgO substrate to show that the emitter is just as effective as a THz radiation source when excited either at $\lambda = 800$ nm or at $\lambda = 1550$ nm by ultrafast laser pulses from a fs fiber laser (pulse width 100 fs, repetition rate 100 MHz). Even with low incident power levels, the Fe/Pt spintronic emitter exhibits efficient generation of THz radiation at both excitation wavelengths. It should be mentioned that there is a linear dependence of the generated THz amplitude on pump power in the low-power excitation regime for both pump wavelengths (see Figure 6). At higher pump powers, there will be a deviation from the linear behavior, as also shown in the study by Yang et al. [23]. Herapath et al. [39] also found that the efficiency of THz generation is essentially flat for excitation by 150 fs pulses with center wavelengths ranging from 900 to 1500 nm, using a CoFeB ferromagnetic layer between adjacent nonmagnetic W and Pt layers. From both experiments, it seems that the crucial factor is the amount of energy that is deposited by the pump pulse in the electronic system and not the details of the involved optical transitions. By further probing the THz emission of Fe/Pt bilayers at $\lambda = 400$ nm [40], the spintronic THz emission efficiency of an optimized spintronic emitter was equal strong as with probing at 800 and 1550 nm. So it still remains independent of the optical pump wavelength. In addition, the efficiency is highly tunable with optical pump power [40]. The reason behind the observed effect is a consequence of the fact that the out of equilibrium transport is done not only by the electrons directly excited by the laser, but also by all the electrons that are excited at intermediate energies due to the scattering of the first-generation electrons. Considering that the electron–electron scattering lifetimes sharply decrease with the energy of the excited electron, the direct impact of high energetic electrons on the transport is expected to be minor at high energy excitation. Instead, the most important impact is that, by scattering with another electron, the electrons will lose energy, they will go down to an intermediate energy and transfer that energy to secondary electrons. This results in an intermediate energy electrons multiplication, which is very similar to a direct excitation by a laser at lower frequency. Even with lower energies now, they will have longer lifetimes and they will contribute to the transport more importantly. If the system is excited with very low-frequency photons, other effects can become important, changing the qualitative scenario mentioned. In this case, one has to take into account that the spin diffusion requires not only asymmetry between the two spin channels, but also between electrons and holes.

4.3.1 Wavelength dependence—summary and outlook

The fact that efficient generation of THz radiation from spintronic structures is possible with lasers over a wide

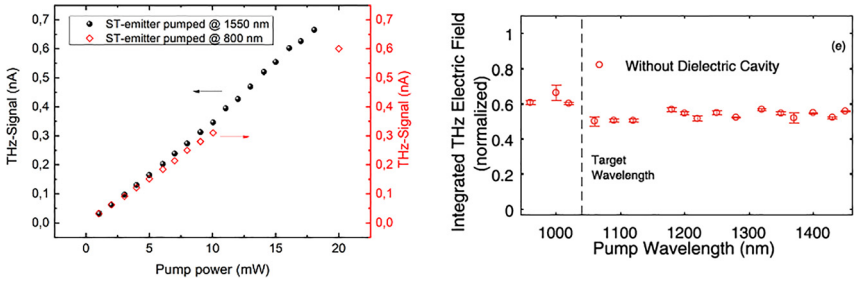

Figure 6: Excitation wavelength dependence of the THz emission.
(Left panel) Maximum THz-E-field as a function of pump power of the laser recorded at 1550 nm (black squares) and 800 nm pump wavelength, $\lambda_{excitation}$. Figure modified from the study by Papaioannou et al. [38], Copyright 2018, IEEE. (Right panel) THz-E-field, emitted from a W/CoFeB/Pt sample as a function of the pump wavelength while the energy, focus diameter and duration of the pump pulses were kept constant. Reprinted from the study by Herapath et al. [39] with the permission of AIP Publishing, Copyright 2019.

wavelength range will have important consequences for the use of such emitters in future applications. For example, the efficient excitation at 1550 nm wavelength allows the immediate integration of such spintronic emitters in THz systems driven by relatively low cost and compact fs-fiber lasers, without the need for frequency conversion. In the future, it will be crucial for the development of efficient spintronic THz emitters to understand the mechanisms of spin current generation and transport at lower and at higher excitation energies also from a theoretical point of view.

4.4 Interface dependence

4.4.1 Interface dependence—structural properties

Even though the transfer of a spin current from a FM to a NM layer (that is, the source of THz emission) is a highly interface-sensitive effect, only few investigations have tried to correlate the structural quality of the interface with the THz signal strength and spectrum. A direct comparison of an epitaxial Fe(3 nm)/Pt(3 nm) bilayer with a signal-optimized polycrystalline CoFeB/Pt structure with the same layer thicknesses revealed a comparable THz signal strength [5]. In contrast, a significant increase in signal amplitude between Fe/Pt emitters grown epitaxially on MgO (100) substrates compared to polycrystalline emitters grown on sapphire substrates was reported by Torosyan et al. [13]. Similarly, the better crystal quality of a CoFeB layer, controlled by the annealing temperature, has significantly enhanced THz emission intensity [41]. Nenno et al. [22] have investigated in detail the performance of spintronic terahertz emitters by modifying the interface quality and its defect density. In particular, the presence of defect density was correlated with the elastic electron-defect scattering lifetime τ_{el} in the FM and NM layers and the interface transmission T for spin-polarized, nonequilibrium electrons. A decreased defect density increases the electron-defect scattering lifetime and this results in a longer-lasting and stronger spin current pulse. Accordingly, a significant enhancement of the THz-signal amplitude and a shift of the spectrum toward lower-THz frequencies [22] were observed, see Figure 7. Furthermore, besides the defect density, the presence of the parameter of the interface transmission T plays an important role. The latter is correlated to the ability of the interface to transfer hot carriers into the NM layer. It was shown [22] that the interface transmission influences the spectral amplitude

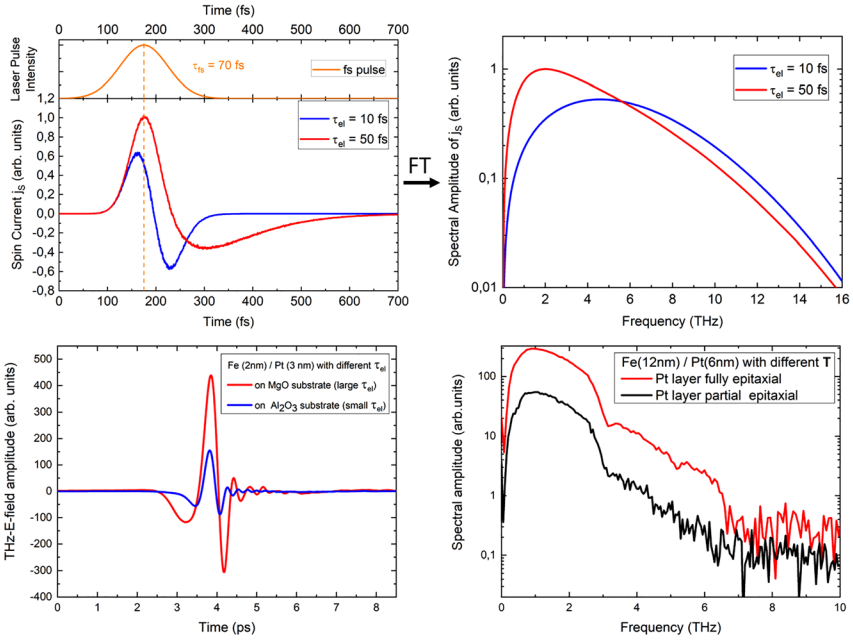

Figure 7: Dependence of the THz emission on the structural quality of the interface.
(Upper panel-Left) Numerical simulations of the Boltzmann transport equation for an Fe/Pt spintronic emitter for different elastic scattering lifetimes τ_{el}. The temporal evolution of the laser pulse intensity with a length of 70 fs is also shown on top. (Upper panel-Right) Spectral amplitude of the simulated spin current (and consequently of the charge current) inside Pt layer obtained by the Fourier transform of the pulses on the left. (Lower panel—Left) Experimental THz-E-field amplitudes for Fe/Pt samples with different τ_{el} as detected after traveling the optical beam path of a THz-TDS setup. (Lower panel—Right) Experimental spectra amplitudes of Fe/Pt heterostructures with different interface transmissions T. Figure modified from the study by Nenno et al. [22].

of the emitted THz field but conserves the composition of the spectrum, see Figure 7.

Similarly, Li et al. [42] showed the decisive role of the microstructural properties of a Co–Pt interface in the THz emission. High interfacial roughness between Co–Pt interface led to a decrease of the THz emission. The introduction of an Co_xPt_{1-x} alloy as a spacer at the Co–Pt interface showed that the intermixing amplified the THz emission. Maximum amplification by a factor of 4.2 was achieved for a $Co_{25}Pt_{75}$(1 nm thick) interlayer. Possible explanation could be the higher flux of spin currents into Pt due to reduction of spin decoherence at the interface caused by the presence of the alloy.

4.4.2 Interface dependence—interlayer

The influence of an interlayer on the THz emission has been also studied. One prominent choice as interlayer is Cu, due to its negligible spin Hall angle and its large spin diffusion length. The strength of the THz signal amplitude was found to decrease with increasing Cu-layer thickness [38], either exponentially [21] or linearly [43]. Interestingly, the spin current relaxation length obtained from thickness dependence studies was revealed to be larger than for metals with sizeable spin Hall effect but, on the other hand, small compared to DC spin-diffusion lengths, that in Cu are of the order of 100 nm [21]. The use of a semiconducting material such as ZnO as interlayer has strongly suppressed the THz signal [43]. The use of insulating interlayers like MgO also strongly suppresses the THz signal. However, the suppression of spin current through MgO can be an advantage in multilayers, as we will see in the next section of geometry dependence.

4.4.3 Interface dependence—summary and outlook

The understanding and the structural engineering of THz intensity and spectral bandwidth of spintronic emitters remains an uncharted territory. First efforts have revealed the defect engineering as a factor that can in future be utilized to shape the THz emission. Nonmagnetic interlayers like Cu, ZnO, MgO lead to a reduction of the emitted radiation in FM/interlayer/NM structures.

4.5 Stack geometry dependence

The geometrical arrangement of the layers can play a decisive role for the THz emission (see Figure 8). Seifert et al. [5] used instead of a FM/NM bilayer a trilayer in the form of NM1/FM/NM2 layers. The special feature of the trilayers is that the NM1 and NM2 layers have opposite spin Hall angles, like W and Pt. In such a way, the spin Hall currents in W and Pt flow in the same direction and radiate in phase and thus enhance the THz amplitude. Large improvement of the signal was achieved in multilayers made of Fe/Pt/MgO [23]. The MgO layer as an insulating layer hinders the flow of the spin current. The spin current can flow from each Fe layer to its neighboring Pt layer and generate THz radiation. Since the transverse charge currents are almost in phase, the THz signal from each layer is added constructively and boost the emission. Maximum signal was observed for 3 repetitions of Fe/Pt/MgO layers while above 3 the detected THz signal dropped, due to the absorption of light. Hibberd et al. [44] followed another route to manipulate the THz radiation. They altered not the layer stack but the magnetic field pattern that is applied to the spintronic source. The goal was to manipulate the magnetic state of the ferromagnetic layer and therefore the polarization profile of the THz radiation. When the spintronic source was placed between two magnets of opposing polarity, THz radiation with a quadrupole-like polarization was generated. When focused, it resulted in longitudinal THz electric field amplitudes twice as much as that of the transverse signals achieved with linearly polarized THz radiation. Ogasawara et al. [45] used synthetic magnets to manipulate the THz radiation. In particular, they prepared NM1(Ta)/CoFeB(FM)/Ir(NM2)/CoFeB(FM)/Ta(NM2) synthetic magnetic multilayers where the Ir spacer had different thicknesses. In such stacking, THz emission is expected when the magnetizations of the CoFeB layers are antiparallel. The authors observed THz emission under no applied magnetic field for samples with antiferromagnetic coupling and oscillations of the signal with respect to Ir thicknesses. In addition, Li et al. [46] showed as a proof-of-concept, the use a magnetic tunnel junction (MTJ) as a THz source. They used a MTJ multistack of Ta/Ru/pinned FM stack/MgO/free FM stack/Ta/Ru. The source of the THz radiation due to the ISHE was the free FM layer/Ta interface while the pinned FM layer controlled the magnetic state of the free FM layer and so the THz signal strength and polarization. A different kind of multilayered structure was examined by Fix et al. [47] composed of ferrimagnetic (FIM) rare-earth-3d transition metal alloys. In particular, the structure had the form of Pt(3 nm)/$Gd_{10}Fe_{90}$(3 nm)/W(3 nm)/$Gd_{30}Fe_{70}$ (3 nm)/Pt(3 nm). The combination of NM-layers with opposite spin Hall angle (Pt, W) with FIM-layers of GdFe with suitable film thickness and composition was utilized to control the terahertz high and low emission state by temperature. Temperature was able to switch the relative alignment of the Fe moments in the different GdFe layers and thus the strength of the THz

emission. Another approach was presented by Feng et al. [48] where the performance of the spintronic THz emitter was improved by utilizing optics. In particular, the work utilized metal (NM1/FM/NM2)-dielectric photonic crystal structure where the metal Pt (1.8 nm)/Fe(1.8 nm)/W (1.8 nm) served as the spintronic emitter and the dielectric interlayers was SiO_2, while the maximum number of layer repeats in the photonic crystal was 3. The goal was to suppress the reflection and transmission of laser light simultaneously aiming to maximize the laser field strength in the metal layers. As a result, the maximization of the laser energy absorption in the metallic emitter improved the conversion efficiency of about 1.7 times compared to a NM1/FM/NM2 single THz emitter. Similarly, one year later, Herapath et al. [39] utilized a dielectric cavity composed of TiO_2 and SiO_2, which was attached on a W/CoFeB/Pt emitter resulting in an enhancement factor of 2 in the THz emission. Chen et al. [49] used a cascade of two spintronic emitters to produce circularly polarized terahertz waves. They used the residual transmitted optical pump power after the first emitter to excite the second-stage emitter. Equal amplitudes were achieved by adjusting the losses of the pump laser in the first emitter. The arrangement of the applied magnetic field directions on both emitters was such that perpendicular electric-field directions were achieved for the terahertz beams generated in the two stages. By adjusting the refractive index difference of low-pressure air between optical and terahertz-frequency ranges, a phase difference between the terahertz waves was introduced in such a way that the mixing of the waves could lead to arbitrary control of the terahertz polarization-shaping, including also the chirality.

4.5.1 Stack geometry dependence—summary and outlook

The trilayer structures NM1/FM/NM2 with the nonmetallic layers of opposite spin Hall angle are proven to be the most efficient spintronic emitters. However, the structural quality of very thin NM is not always guaranteed. The studies on optical-assisted THz generation using photonic crystals have just started. The idea of manipulating the magnetization direction of the FM layer, either by creating external magnetic field patterns or manipulating the magnetic state of the magnetic layers like in synthetic magnets, is very effective and interesting from physics and technological point of view. The future investigation of the stack geometry would definitely include manipulation of magnetic state of the FM layer in different giant magnetoresistance (GMR) and tunnel magnetoresistance (TMR) structures. Application of field patterns and multilayers structure can be very useful for enhancing and shaping of the THz emission. After all, the concept of modifying the stack geometry by means of geometrical and magnetic order holds big promises for future designs of tunable THz emitters.

5 Future perspectives of THz spintronic emitters

THz spintronic emitters are certainly a new direction in physics with a huge potential for technological applications. They define the new field of ultrafast terahertz optospintronics. The emitters have many advantages: they are of low cost, ultrabroadband, easy to use and robust.

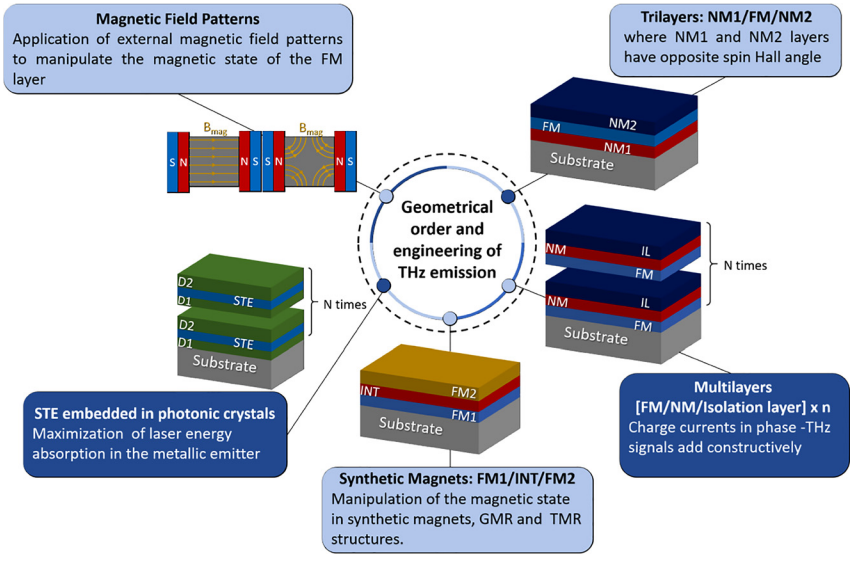

Figure 8: Graphical representation of geometrical stacking order that can influence the intensity, bandwidth and the polarization state of the emitted THz signals. FM denotes the ferromagnetic layer, NM the nonmagnetic layer, IL the isolation layer, STE is the spintronic emitter, D1,2 the dielectric layers and INT the interlayer in synthetic magnetic structures.

The performance of the emitters is comparable to state-of-the-art terahertz sources like the ones routinely used to cover the range from 0.3 to 8 THz, the nonlinear optical crystals like ZnTe (110), GaP and high-performance photoconductive switches [5]. The challenge nowadays is to generate THz broadband radiation with sufficient power. In this direction, Seifert et al. [50] explored the up-scaling capabilities of metallic spintronic stacks in order to achieve intense THz sources. They used large area W/CoFeB/Pt stack of 5.6 nm thickness.

The emitted THz pulse was found to reach energies of 5 nJ with peak field values of up to 300 $kVcm^{-1}$ when excited with a laser pulse energy of 5.5 mJ. This corresponds to a conversion efficiency of 10^{-6}. Similar conversion efficiencies were reported for high repetition rate systems with repetition rates of 100 MHz and moderate average powers (up to 500 mW) using Fe/Pt bilayers [38]. The estimated absolute average power of the generated THz pulses was almost 50 μW for a pump power of 500 mW using 800 nm excitation wavelength. Taking into account a THz pulse length of approximately 1 ps, this corresponds to a comparable conversion efficiency.

Currently, the down-scaling through nanopatterning of the emitters is under investigation. In one of the first investigations on patterned emitters by Yang et al. [23], Fe/Pt heterostructures were patterned in stripes of 5 μm width and a spacing of 5 μm and measurements were performed with the magnetic field along and perpendicular to the stripes. Anisotropic emission was observed with higher intensity for the perpendicular configuration and a blue shift in frequency compared to the parallel configuration. Further, modulation of THz radiation in terms of magnitude, bandwidth and center frequency was achieved based on W/CoFeB/Pt stripe patterns [51]. The patterns had dimensions of 5 μm width and 5 μm spacing (see Figure 9, upper panel). By changing the angle between the applied magnetic field and the stripe direction, modulation of the THz emission was measured. Interestingly, Jin et al. [51] attributed this effect to nanoconfinement of the charge current due to nanopatterning. For a specific configuration of stripe and magnetic field at 90°, the spatial separation of the photo-induced positive and negative charges accumulate and then create a nonequilibrium electric potential $U(t)$ at the edge of the stripe. The transient potential creates an opposite built-in electric field. The latter induces a back flowing current, changes the effective length of the charge flowing and so alters the THz emission. Song et al. [52] fabricated CoFeB/Pt patterned as rectangles and orthogonal structures of 20 μm width and various lengths L, of 20, 40, 80, 160 and 320 μm, while the separation between the elements was 10 μm (see Figure 9, lower panel). They observed a reshaping of the THz wavefront, which indicates that the pattern structure influences the temporal distribution of the transient dynamics of the charge current. The FWHM decreased by decreasing L pointing to the backflow effect as mentioned before, while the center frequency increases by decreasing L as a result of the antenna effect of the microstructures, where it is expected that shorter antennas will lead to higher oscillation frequencies. Microfabricated spintronic emitters were also studied by Wu et al. [53]. Fe (3 nm)/Pt (3 nm) bilayers were patterned by optical lithography in the form of stripes of constant separation of 510 μm and a variable width of 240, 300, 400 and 490 μm. The THz waveform was modulated by the different stripe widths. As the stripe width is reduced, a second peak in the spectra appears, showing that the bandwidth can be increased in such microstructures. Wu et al. interpreted the results in terms of a simplified multislit interference model, which can be a useful tool for designing future patterned emitters. Another approach in patterning was followed by Nandi et al. [54] where the spintronic trilayer of W (2 nm)/CoFeB (1.8 nm)/Pt (2 nm) was inserted in the gap of two antenna types: a slotline (with spacing of 25 μm) and an H-type dipole antenna (with length of 200 μm and gap size of 10 μm). Such antennas are frequently used to improve the radiation efficiency in the state-of-the-art semiconductor-based photoconductive THz emitters and receivers. The coupling between the spintronic emitter and the antennas led to a significant increase in the THz signal compared to plain continuous film emitters. The incorporation of spintronic emitters with already existing THz technologies can drive the on-chip application of this new class of THz emitters based on ultrafast spin and charge currents. In conclusion, the first studies in nanopatterned emitters revealed the ability to modify the THz emission, rendering nanostructuring as a key ingredient for future applications of THz emitters. Meanwhile the first implementation of spintronic emitters in real applications has been realized. Arrays of W/Fe/Pt were proposed to form a THz near-field microscope capable of illuminating an object at an extreme near field [55]. Guo et al. [56] examined the possibility to integrate W/CoFeB/Pt heterostructures in laser terahertz emission microscopy (LTEM) technique. Müller et al. [57] have demonstrated efficient coupling of THz-pulses emitted from W/CoFeB/Pt trilayer to the junction of a scanning tunneling microscope, that has the potential to enable spatiotemporal imaging with femtosecond temporal and sub-nm spatial resolution.

Certainly, future investigations will deal with THz emission from giant magnetoresistance (GMR) and tunnel magnetoresistance (TMR) structures, where the potential

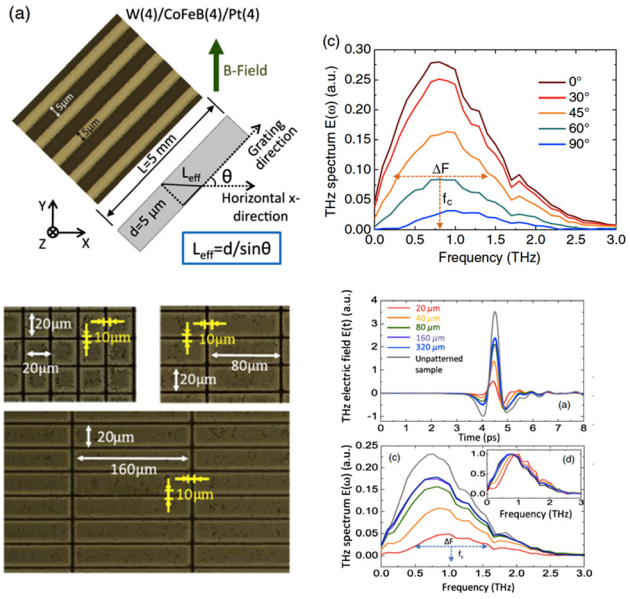

Figure 9: (Upper panel) Illustration of the patterned W/CoFeB/Pt film in stripes of 5 μm width and length. Shift of the central frequency and changes in the FWHM are observed for different orientations between stripes and external magnetic field. Reproduced from the study by Jin et al. [51] with permission of Wiley-VCH, Copyright 2019. (Lower panel) Blocky patterned CoFeB/Pt with lengths ranging from 20 to 160 μm. Shaping of the THz spectral amplitude is observed for different patterned dimensions. Reproduced from the study by Song et al. [52] with permission of The Japan Society of Applied Physics, Copyright 2019.

for THz manipulation by defining the magnetic states of the layers is large. Open challenges for the coming years are the use of spintronic structures as detectors of THz radiation, the exploration of appropriate materials, interfaces and nanopatterns, the electrical detection of the ultrashort current pulses, and the use of emission for microscopy and imaging in the near- and far-field.

6 Conclusion

Spintronic emitters can cover a frequency range from 0.1 to well above 30 THz without phonon absorption of the emitter material. The latter renders them superior to all the current solid-state emitters. The big challenge nowadays is to generate broadband THz radiation with sufficient power by appropriate combination of materials, multilayer stacks, growth quality and nanopatterning. The use of such sources in THz-imaging has just launched. The physics of the optospintronic phenomena can shed light on many light-induced magnetic interactions. The field is still in its infancy and the research on the design and control of THz waves emitted from spintronic structures has brilliant perspectives.

Acknowledgement: Garik Torosyan and Laura Scheuer are acknowledged for their long standing collaboration. Philipp Trempler, Nikos Kanistras and Georg Schmidt are acknowledged for their support on this work. Deutsche Forschungsgemeinschaft (DFG) in the collaborative research center TRR227, project B02 is also acknowledged.

Author contributions: All the authors have accepted responsibility for the entire content of this submitted manuscript and approved submission.

Research funding: This research was funded by Deutsche Forschungsgemeinschaft (DFG) in the collaborative research center TRR227.

Conflict of interest statement: The authors declare no conflicts of interest regarding this article.

References

[1] B. Ferguson and X.-C. Zhang, "Materials for terahertz science and technology," *Nat. Mater.*, vol. 1, pp. 26–33, 2002.

[2] D. M. Mittleman, "Perspective: terahertz science and technology," *J. Appl. Phys.*, vol. 122, p. 230901, 2017.

[3] M. Tonouchi, "Cutting-edge terahertz technology," *Nat. Photonics*, vol. 1, pp. 97–105, 2007.

[4] T. Kampfrath, M. Battiato, P. Maldonado, et al., "Terahertz spin current pulses controlled by magnetic heterostructures," *Nat. Nanotechnol.*, vol. 8, p. 256, 2013.

[5] T. Seifert, S. Jaiswal, U. Martens, et al., "Efficient metallic spintronic emitters of ultrabroadband terahertz radiation," *Nat. Photonics*, vol. 10, pp. 483–488, 2016.

[6] R. A. Lewis, "A review of terahertz sources," *J. Phys. Appl. Phys.*, vol. 47, p. 374001, 2014.

[7] E. Beaurepaire, G. M. Turner, S. M. Harrel, M. C. Beard, J.-Y. Bigot, and C. A. Schmuttenmaer, "Coherent terahertz emission from ferromagnetic films excited by femtosecond laser pulses," *Appl. Phys. Lett.*, vol. 84, pp. 3465–3467, 2004.

[8] D. J. Hilton, R. D. Averitt, C. A. Meserole, et al., "Terahertz emission via ultrashort-pulse excitation of magnetic metal films," *Opt. Lett.*, vol. 29, pp. 1805–1807, 2004.

[9] M. Battiato, K. Carva, and P. M. Oppeneer, "Superdiffusive spin transport as a mechanism of ultrafast demagnetization," *Phys. Rev. Lett.*, vol. 105, p. 027203, 2010.

[10] J. Hurst, P.-A. Hervieux, and G. Manfredi, "Spin current generation by ultrafast laser pulses in ferromagnetic nickel films," *Phys. Rev. B*, vol. 97, p. 014424, 2018.

[11] G. Manfredi and P. A. Hervieux, "Finite-size and nonlinear effects on the ultrafast electron transport in thin metal films," *Phys. Rev. B*, vol. 72, p. 155421–13, 2005.

[12] D. M. Nenno, R. Binder, and H. C. Schneider, "Simulation of hot-carrier dynamics and terahertz emission in laser-excited metallic bilayers," *Phys. Rev. Appl.*, vol. 11, p. 054083, 2019.

[13] G. Torosyan, S. Keller, L. Scheuer, R. Beigang, and E. T. Papaioannou, "Optimized spintronic terahertz emitters based on epitaxial grown Fe/Pt layer structures," *Sci. Rep.*, vol. 8, p. 1311, 2018.
[14] W. Zhang, P. Maldonado, Z. Jin, et al., "Ultrafast terahertz magnetometry," *Nat. Commun.*, vol. 11, p. 4247, 2020.
[15] C. Zhou, Y. P. Liu, Z. Wang, et al., "Broadband terahertz generation via the interface inverse rashba-edelstein effect," *Phys. Rev. Lett.*, vol. 121, p. 086801, 2018.
[16] M. B. Jungfleisch, Q. Zhang, W. Zhang, et al., "Control of terahertz emission by ultrafast spin-charge current conversion at Rashba interfaces," *Phys. Rev. Lett.*, vol. 120, p. 207207, 2018.
[17] Q. Zhang, Z. Luo, H. Li, Y. Yang, X. Zhang, and Y. Wu, "Terahertz emission from anomalous Hall effect in a single-layer ferromagnet," *Phys. Rev. Appl.*, vol. 12, p. 054027, 2019.
[18] C. Fattinger and D. Grischkowsky, "Terahertz beams," *Appl. Phys. Lett.*, vol. 54, pp. 490–492, 1989.
[19] P. U. Jepsen, R. H. Jacobsen, and S. R. Keiding, "Generation and detection of terahertz pulses from biased semiconductor antennas," *J. Opt. Soc. Am. B*, vol. 13, pp. 2424–2436, 1996.
[20] M. Chen, R. Mishra, Y. Wu, K. Lee, and H. Yang, "Terahertz emission from compensated magnetic heterostructures," *Adv. Opt. Mater.*, vol. 6, p. 1800430, 2018.
[21] T. S. Seifert, N. M. Tran, O. Gueckstock, et al., "Terahertz spectroscopy for all-optical spintronic characterization of the spin-Hall-effect metals Pt, W and Cu80Ir20," *J. Phys. Appl. Phys.*, vol. 51, p. 364003, 2018.
[22] D. M. Nenno, L. Scheuer, D. Sokoluk, et al., "Modification of spintronic terahertz emitter performance through defect engineering," *Sci. Rep.*, vol. 9, p. 13348, 2019.
[23] D. Yang, J. Liang, C. Zhou, et al., "Powerful and tunable THz emitters based on the Fe/Pt magnetic heterostructure," *Adv. Opt. Mater.*, vol. 4, pp. 1944–1949, 2016.
[24] Y. Sasaki, Y. Kota, S. Iihama, K. Z. Suzuki, A. Sakuma, and S. Mizukami, "Effect of Co and Fe stoichiometry on terahertz emission from Ta/$(Co_xFe_{1-x})_{80}B_{20}$/MgO thin films," *Phys. Rev. B*, vol. 100, p. 140406, 2019.
[25] R. Schneider, M. Fix, R. Heming, S. Michaelis de Vasconcellos, M. Albrecht, and R. Bratschitsch, "Magnetic-field-dependent THz emission of spintronic TbFe/Pt layers," *ACS Photonics*, vol. 5, pp. 3936–3942, 2018.
[26] R. Schneider, M. Fix, J. Bensmann, S. Michaelis de Vasconcellos, M. Albrecht, and R. Bratschitsch, "Spintronic GdFe/Pt THz emitters," *Appl. Phys. Lett.*, vol. 115, p. 152401, 2019.
[27] T. Seifert, U. Martens, S. Günther, et al., "Terahertz spin currents and inverse spin Hall effect in thin-film heterostructures containing complex magnetic compounds," *SPIN*, vol. 57, p. 1740010, 2017.
[28] Y. Sasaki, Y. Takahashi, and S. Kasai, "Laser-induced terahertz emission in Co2MnSi/Pt structure," *APEX*, vol. 13, p. 093003, 2020.
[29] Y. Wu, M. Elyasi, X. Qiu, et al., "High-performance THz emitters based on ferromagnetic/nonmagnetic heterostructures," *Adv. Mater.*, vol. 29, p. 1603031, 2017.
[30] S. Zhang, Z. Jin, Z. Zhu, et al., "Bursts of efficient terahertz radiation with saturation effect from metal-based ferromagnetic heterostructures," *J. Phys. Appl. Phys.*, vol. 51, p. 034001, 2017.
[31] J. Cramer, T. Seifert, A. Kronenberg, et al., "Complex terahertz and direct current inverse spin Hall effect in YIG/Cu1–xIrx bilayers across a wide concentration range," *Nano Lett.*, vol. 18, pp. 1064–1069, 2018.
[32] T. S. Seifert, S. Jaiswal, J. Barker, et al., "Femtosecond formation dynamics of the spin Seebeck effect revealed by terahertz spectroscopy," *Nat. Commun.*, vol. 9, p. 2899, 2018.
[33] L. Cheng, X. Wang, W. Yang, et al., "Far out-of-equilibrium spin populations trigger giant spin injection into atomically thin MoS2," *Nat. Phys.*, vol. 15, pp. 347–351, 2019.
[34] N. H. D. Khang, Y. Ueda, and P. N. Hai, "A conductive topological insulator with large spin Hall effect for ultralow power spin–orbit torque switching," *Nat. Mater.*, vol. 17, pp. 808–813, 2018.
[35] X. Wang, L. Cheng, D. Zhu, et al., "Ultrafast spin-to-charge conversion at the surface of topological insulator thin films," *Adv. Mater.*, vol. 30, p. 1802356, 2018.
[36] T. H. Dang, J. Hawecker, E. Rongione, et al., "Ultrafast spin-currents and charge conversion at 3d-5d interfaces probed by time-domain terahertz spectroscopy," *Appl. Phys. Rev.*, vol. 7, no. 4, p. 041409, 2020.
[37] H. S. Qiu, K. Kato, K. Hirota, N. Sarukura, M. Yoshimura, and M. Nakajima, "Layer thickness dependence of the terahertz emission based on spin current in ferromagnetic heterostructures," *Opt. Express*, vol. 26, pp. 15247–15254, 2018.
[38] E. T. Papaioannou, G. Torosyan, S. Keller, et al., "Efficient terahertz generation using Fe/Pt spintronic emitters pumped at different wavelengths," *IEEE Trans. Magn.*, vol. 54, pp. 1–5, 2018.
[39] R. I. Herapath, S. M. Hornett, T. S. Seifert, et al., "Impact of pump wavelength on terahertz emission of a cavity-enhanced spintronic trilayer," *Appl. Phys. Lett.*, vol. 114, p. 041107, 2019.
[40] R. Beigang, E. T. Papaioannou, L. Scheuer, et al., "Efficient terahertz generation using Fe/Pt spintronic emitters pumped at different wavelengths," in *Terahertz, RF, Millimeter, and Submillimeter-wave Technology and Applications XII*, vol. 10917, L. P. Sadwick and T. Yang, Eds., San Francisco, International Society for Optics and Photonics (SPIE), 2019, pp. 74–80.
[41] Y. Sasaki, K. Z. Suzuki, and S. Mizukami, "Annealing effect on laser pulse-induced THz wave emission in Ta/CoFeB/MgO films," *Appl. Phys. Lett.*, vol. 111, p. 102401, 2017.
[42] G. Li, R. Medapalli, R. V. Mikhaylovskiy, et al., "THz emission from Co/Pt bilayers with varied roughness, crystal structure, and interface intermixing," *Phys. Rev. Mater.*, vol. 3, p. 084415, 2019.
[43] G. Li, R. V. Mikhaylovskiy, K. A. Grishunin, J. D. Costa, T. Rasing, and A. V. Kimel, "Laser induced THz emission from femtosecond photocurrents in Co/ZnO/Pt and Co/Cu/Pt multilayers," *J. Phys. Appl. Phys.*, vol. 51, p. 134001, 2018.
[44] M. T. Hibberd, D. S. Lake, N. A. B. Johansson, T. Thomson, S. P. Jamison, and D. M. Graham, "Magnetic-field tailoring of the terahertz polarization emitted from a spintronic source," *Appl. Phys. Lett.*, vol. 114, p. 031101, 2019.
[45] Y. Ogasawara, Y. Sasaki, S. Iihama, A. Kamimaki, K. Z. Suzuki, and S. Mizukami, "Laser-induced terahertz emission from layered synthetic magnets," *APEX*, vol. 13, p. 063001, 2020.
[46] J. Li, Z. Jin, B. Song, et al., "Magnetic-field-free terahertz emission from a magnetic tunneling junction," *Jpn. J. Appl. Phys.*, vol. 58, p. 090913, 2019.

[47] M. Fix, R. Schneider, J. Bensmann, S. Michaelis de Vasconcellos, R. Bratschitsch, and M. Albrecht, "Thermomagnetic control of spintronic THz emission enabled by ferrimagnets," *Appl. Phys. Lett.*, vol. 116, p. 012402, 2020.
[48] Z. Feng, R. Yu, Y. Zhou, et al., "Highly efficient spintronic terahertz emitter enabled by metal–dielectric photonic crystal," *Adv. Opt. Mater.*, p. 1800965, 2018, https://doi.org/10.1002/adom.201800965.
[49] X. Chen, X. Wu, S. Shan, et al., "Generation and manipulation of chiral broadband terahertz waves from cascade spintronic terahertz emitters," *Appl. Phys. Lett.*, vol. 115, p. 221104, 2019.
[50] T. Seifert, S. Jaiswal, M. Sajadi, et al., "Ultrabroadband single-cycle terahertz pulses with peak fields of 300 kV/cm from a metallic spintronic emitter," *Appl. Phys. Lett.*, vol. 110, p. 252402, 2017.
[51] Z. Jin, S. Zhang, W. Zhu, et al., "Terahertz radiation modulated by confinement of picosecond current based on patterned ferromagnetic heterostructures," *Phys. Status Solidi Rapid Res. Lett.*, vol. 13, p. 1900057, 2019.
[52] B. Song, Y. Song, S. Zhang, et al., "Controlling terahertz radiation with subwavelength blocky patterned CoFeB/Pt heterostructures," *APEX*, vol. 12, p. 122003, 2019.
[53] W. Wu, S. Lendinez, M. Taghipour Kaffash, R. D. Schaller, H. Wen, and M. B. Jungfleisch, "Modification of terahertz emission spectrum using microfabricated spintronic emitters," *J. Appl. Phys.*, vol. 128, p. 103902, 2020.
[54] U. Nandi, M. S. Abdelaziz, S. Jaiswal, et al., "Antenna-coupled spintronic terahertz emitters driven by a 1550 nm femtosecond laser oscillator," *Appl. Phys. Lett.*, vol. 115, p. 022405, 2019.
[55] S.-C. Chen, Z. Feng, J. Li, et al., "Ghost spintronic THz-emitter-array microscope," *Light Sci. Appl.*, vol. 9, p. 99, 2020.
[56] F. Guo, C. Pandey, C. Wang, et al., "Generation of highly efficient terahertz radiation in ferromagnetic heterostructures and its application in spintronic terahertz emission microscopy (STEM)," *OSA Continuum*, vol. 3 pp. 893–902, 2020.
[57] M. Müller, N. Martín Sabanés, T. Kampfrath, and M. Wolf, "Phase-resolved detection of ultrabroadband THz pulses inside a scanning tunneling microscope junction," *ACS Photonics*, vol. 7, pp. 2046–2055, 2020.